International Journal of Thermofluids 22 (2024) 100659

Contents lists available at ScienceDirect

International Journal of Thermofluids

journal homepage: www.sciencedirect.com/journal/international-journal-of-thermofluids

Heat transfer in a vessel-tubes array with a rotating baffle: A rotating frame modeling approach

Ali Q. Abd Al-Hasan [a], Muneer A. Ismael [a,b,*], Mohammad Ghalambaz [c]

[a] Mechanical Engineering Department, College of Engineering, University of Basrah, Basrah, Iraq
[b] College of Engineering, University of Warith Al-Anbiyaa, Karbala, Iraq
[c] Laboratory on Convective Heat and Mass Transfer, Tomsk State University 634045 Tomsk, Russia

ARTICLE INFO

Keywords:
Heat transfer enhancement
Rotating frame
Mixer
Heat exchanger
Rotating mesh

ABSTRACT

Conveying heat from one medium to another is more critical when merging these media is banned. Thus, the media should flow individually in separate pipes. This paper explores the exchange of heat between tube bundles enclosed in a circular vessel with a rotating frame. The rotating frame serves to modulate the natural convection to mixed convection. The hot and cold tubes are distributed peripherally while the rotor is centered in the insulated vessel. The study focused on the configuration of the tubes, namely their number, size (r^*), and radial position (e^*), and how these parameters act with various Rayleigh numbers ($Ra = 10^3$ - 10^5) and rotational speeds ($\omega^* = 0$ - 400). The time-dependent equations are discretized and solved using the finite element method with rotating meshes. The outcomes indicate that the augmentation of Nusselt number with the rotational speed and Rayleigh number relies significantly on the radial position, the size as well as the number of hot tubes. The Nusselt number increases by 74.59 % and 9.57 % for $Ra = 10^5$ and 10^3, respectively, when the rotational speed is elevated from 0 to 200, whereas it increases by 308 % when the tube size is reduced from $r^* = 0.05$ to $r^* = 0.01$ at $\omega^* = 200$. It is deduced that the size of the tube is the supreme parameter affecting the Nusselt number.

1. Introduction

Many researchers have been interested in studying the heat transfer and velocity of the mixed flow of enclosure with a rotating cylinder due to its prevalence in various engineering applications such as heat exchangers, nuclear and chemical reactors [1,2], electronic cooling systems as well as solar energy [3]. In order to examine enclosures with and without rotating or stationary obstacles, several computational and experimental techniques have been created. Many investigators dealt with theoretical rotating (elliptic and square cylinder). The elliptical cylinder is illustrated in [4–6]. Zhang *et al.* [4] performed a numerical study of free convection in a square-shaped enclosure containing a heated elliptic-shaped cylinder. The change in the Rayleigh number from 10^3 to 10^6 and the square area's slope from 0° to 45° were used. It was found that the Rayleigh number has an apparent effect on streamlines and isotherms lines. They noted little impact on the rates of Nusselt numbers relative to the hot elliptic cylinder at the inclination of the square enclosure. Karbasifar *et al.* [5] illustrated the mixed convection inside a cavity containing an elliptic-shaped cylinder using a nanofluid, which is water-aluminum oxide. Richardson numbers are taken from 0.01 to 100. It was shown that the Richardson increase leads to a negative effect on the rates of Nusselt numbers. Seo *et al.* [6] implemented a three-dimensional numerical study of free convection within a rectangular enclosure containing a hot cylinder in the middle. In this study, two forms of cylinders were used, the circular and elliptic cylinders, and the results were compared between them. The results were found at the Rayleigh number at 10^6. When the radii of the cylinder and the elliptic shape are equal to 0.4 times the length of the enclosure, the percentage increase in the average Nusselt numbers for the cylindrical shape is 34.77 %, and for the elliptic shape is 35.86 %.

A few studies have focused on two rotating cylinders placed within an enclosure. For instance, Park *et al.* [7] numerically studied two hot rotating cylinders inside an enclosure. They reported that putting these two cylinders at the top results in a better heat transfer rate. Most of the researchers used one rotating cylinder inside the enclosure. Ghaddar and Thiele [8] assessed the influence of heat transfer by a horizontal cylinder rotating around the center and within an enclosure. This study found that when the ratio of the Rayleigh number to the square of the Reynolds number decreases, the maximum temperature on the surface of the cylinder decreases by 25 %–35 %. Ghaddar [9] directed her effort on the mixed load within a rectangular enclosure containing a rotating

---

* Corresponding author.
E-mail address: muneer.ismael@uobasrah.edu.iq (M.A. Ismael).

https://doi.org/10.1016/j.ijft.2024.100659
Received 19 February 2024; Received in revised form 29 March 2024; Accepted 10 April 2024
Available online 13 April 2024

Nomenclature

a	Height of the rotating frame, m
b	Width of the rotating frame, m
C_p	Constant pressure specific heat, J $kg^{-1}K^{-1}$
D	Diameter of the vessel (2R), m
D_h	Hydraulic diameter, m
e	The distance from the center of the vessel to the center of the hot tube, m
$\overrightarrow{F}_b$	Buoyant force vector, N
g	Gravitational acceleration, m s^{-2}
k	Thermal conductivity, W $m^{-1}K^{-1}$
k_f	Thermal conductivity of the fluid, W $m^{-1}K^{-1}$
k_s	Thermal conductivity of the solid, W $m^{-1}K^{-1}$
n	Normal vector
N	Number of hot and cold tubes
Nct	Number of cold tubes
Nht	Number of hot tubes
Nu	Nusselt number, dimensionless
p	Pressure, N m^{-2}
Pr	Prandtl number, dimensionless
r	Radius of the heater, m
R	Radius of the vessel, m
Ra	Rayleigh number, dimensionless
Re	Reynold number, dimensionless
R_h	Heat capacity ratio,
$R_{th.}$	Thermal conductivity ratio,
t	Time, s
T	Temperature, K
u, v	Velocities, dimensional m s^{-1}
$\overrightarrow{V}$	Absolute velocity vector, m s^{-1}
$\overrightarrow{W}$	Relative velocity vector, m s^{-1}
x, y	Cartesian co- ordinates, m

Greek Symbols

ΔT	Temperature difference, K
α	Thermal diffusivity, $m^2.s^{-1}$
β	Coefficient of thermal expansion of fluid, K^{-1}
θ	Dimensionless temperature, $\theta = \frac{(T-T_h)}{(T_c-T_h)}$
μ	Dynamic viscosity, kg.$m^{-1}.s^{-1}$
ρ	Density, kg m^{-3}
υ	Kinematic viscosity of the fluid, m^2 s^{-1}
ω	Angular velocity of the frame, rad s^{-1}
$\overrightarrow{\omega}$	Angular velocity vector of the frame, rad s^{-1}
ε	Angle
ε_1	Angle between the x-axis and center of the tube
ε_2	Angle between two of tubes center

Subscripts

c	Cold (lower value)
f	Fluid
h	Hot (higher value)
j	Unit vector along y axis
s	Solid
0	Reference value, at the center of the vessel

Supersubscript

*	Dimensionless

Abbreviation

FEM	Finite Element Method
PARDISO	Parallel Direct Solver

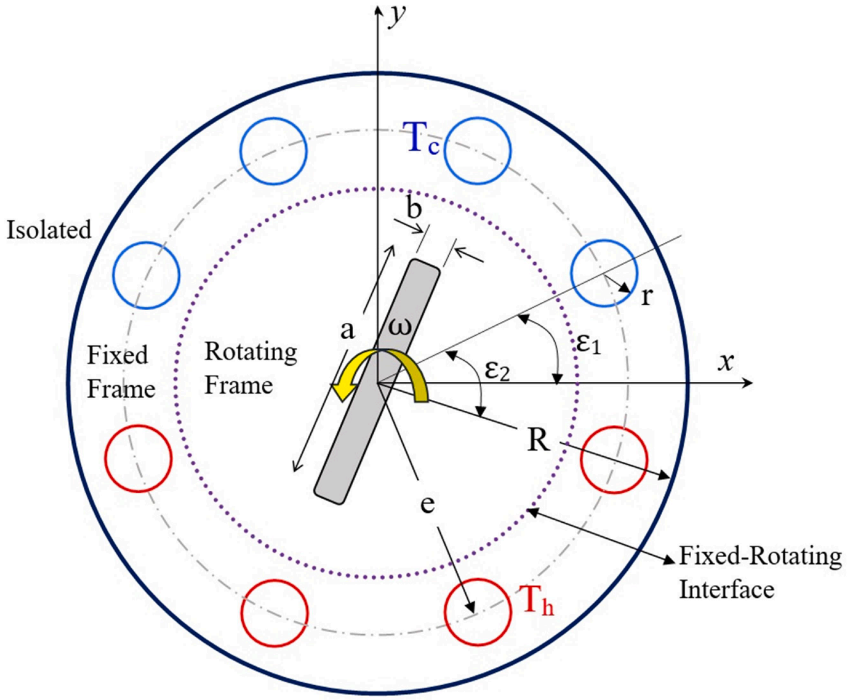

Fig. 1. Schematic configuration and coordinate system of the considered problem.

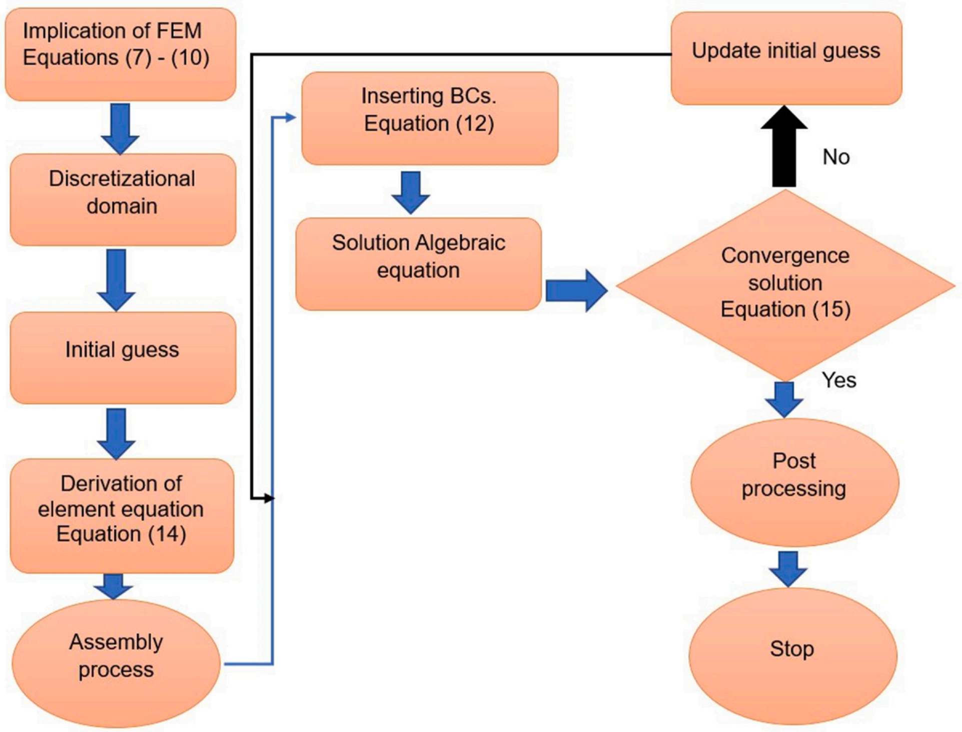

Fig. 2. FEM procedure outline.

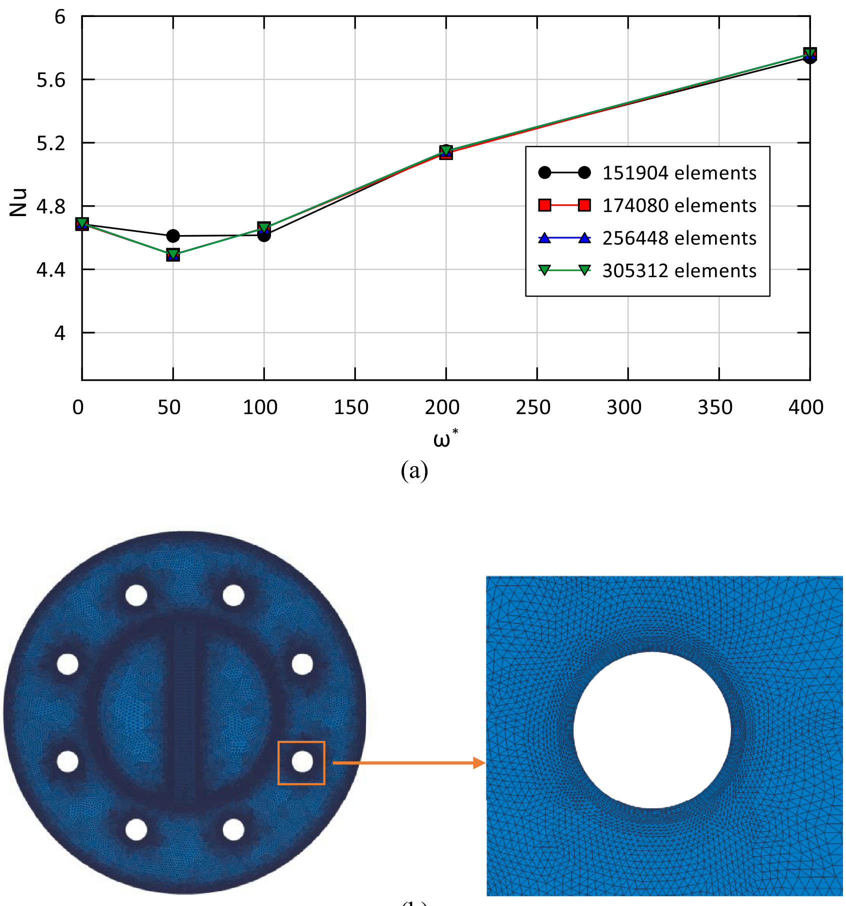

(a)

(b)

Fig. 3. (a) Grid dependency test with different values of ω* for Ra = 10^3, e* = 0.35, Nht = 4, Nct = 4, and r* = 0.03 (b) A portrayed image to the adopted mesh size, 174,080 elements.

Table 1
Compression of the mean Nusselt number with Costa and Raimundo [16] for Ra = 10^5, $R_h = 1$, $R_{th.} = 1$, Pr = 0.6, $R^* = 0.2$ for different rotational speeds.

ω*	Present	Costa and Raimundo [16]	% Error
−500	4.330	4.34	−0.23
−400	4.349	4.34	0.20
−300	4.382	4.36	0.49
−200	4.436	4.40	0.82
−100	4.446	4.47	−0.54
0	4.520	4.55	−0.65
100	4.504	4.54	−0.79
200	4.459	4.48	−0.46
300	4.422	4.44	−0.40
400	4.387	4.37	0.39
500	4.322	4.30	0.50

circular cylinder. Different positions were taken for this rotating cylinder inside the enclosure, and the results showed that the average Nusselt number decreases when that cylinder moves toward the top. Morales *et al.* [10] suggested a Nusselt number correlation for the combined convection of a rotating cylinder inside a square enclosure. This connection provided the heat transfer coefficient of the rotation regime with an error rate of less than 4 %.

Sadeghipour *et al.* [11] showed the effect of a circular rotating cylinder confined by two vertical walls on the rate of heat transfer. The results showed that the greater the distance relative to the distance of those two walls, the higher the heat transfer rate. Yan and Zu [12] adopted the lattice Boltzmann technique to simulate a viscous fluid's flow past an isothermal rotating cylinder with heat transfer. The outcome indicated a rise in the lift coefficient but a decrease in the drag coefficient. Singh and Pop [13] performed a numerical study of the mixed convection of a rotating vertical thin cylinder under the buoyancy force and thermal diffusivity by the intake and injection methods. The results showed that the external surface friction strongly depends on the buoyancy force due to the effects of thermal diffusion and the relative velocity between the wall and the free stream. Ghazanfarian and Nobari [14] studied the effect of fluctuation in the flow by taking a set of Reynolds numbers and Prandtl numbers on the streamlines and isotherm lines. It was found that it is similar to the fixed cylinder. When the rotational speed is increased, the Nusselt number and drag coefficient rates decrease. Paramane and Sharma [15] focused on the effect of a rotating cylinder in a square enclosure. It was found that the average Nusselt number rises with the growth in the Reynolds numbers and declines with the rise in the rotational speed. Costa and Raimundo [16] studied the convection in a square enclosure with a circular cylinder positioned in the center. Two directions of rotation of the cylinder were tested, and a total of the sizes of the circular cylinder were taken by controlling its radius and its effect on streamlines and isotherms lines. The total Nusselt numbers were calculated and found to be linear with the speed of rotation of the cylinder, as they are low when the radius is large, and the rotation is slight, but they increase with that rotation.

Hussain *et al.* [17] addressed numerical simulations within a square enclosure and a circular cylinder with variable locations to see its effect on the rate of heat transfer. Their study considered the Richardson number and the Reynolds numbers, and it found that the Nusselt number increases with these two numbers. In addition to that, changing the location of the rotating cylinder inside the cavity showed a significant effect on heat transfer. Liao and Lin [18] studied the effect of Rayleigh numbers, Richardson numbers, and Prandtl numbers on a domain containing a rotating cylinder. The results concluded that conduction dominates the heat transfer when the Rayleigh number is around 10^4. In addition, the average Nusselt number decreases with the Richardson number decrease. Wang *et al.* [19] used a hot rotating cylinder within an enclosure, showing the influence of Bejan number and total entropy generation. It was found that the rates of the Bejan number decreases with the Reynolds number, the Richardson number, and the irreversibility distribution ratio, and it is constant when the Richardson number is less than unity. On the contrary, the rate of entropy generation increases with these parameters.

A mixed convection study in a lid-driven cavity was conducted by Khanafer *et al.* [20] with a rotating cylinder using the direction of rotation with the variable Richardson numbers. The results showed that the rates of the Nusselt number are highly dependent on the direction of the angular velocity. Luo *et al.* [21] have built the electro-thermo-convection of a completely insulating liquid between a square enclosure and a heated inner circular cylinder by the lattice Boltzmann approach. It was discovered that the heat transfer due to the electrical effect is considerable when the electric driving of the ratio between the Coulomb and shear forces is above a critical level. A numerical exploration of periodic, unstable mixed convective flow and heat transfer within a square enclosure influenced by a centrally rotating circular cylinder has been conducted by Wang *et al.* [22]. The numerical findings demonstrated that the pulsing temperature of the inner cylinder has a significant impact on fluid flow and heat transmission. The heat transmission is typically improved for time-periodic unstable mixed convection compared to steady-state mixed convection. Ismael *et al.* [23] used a rotating hot cylinder within an annular porous medium within a space. It was found that the rotation of the cylinder reduces the Nusselt number, but it contributes significantly to the heat uniformity of the surface of the cylinder. Also, the porous layer and the rotation of the cylinder slightly increased the pressure drop.

Other studies considered the non-Newtonian fluid with the rotation of the cylinder as an attempt to understand the role of cylinder rotation [24–26]. Under the effects of magnetic inclination, Selimefendigil *et al.* [24] investigated a partially heated cavity featuring a rotating cylinder that is adiabatically maintained. Richardson and Hartmann numbers, velocity, and inclination angle of the magnet were investigated. The fluid used is non-Newtonian. The results showed that when the Richardson number is increased, the average heat transfer is improved from the pseudo-plastic fluid and deteriorates with the dilatant fluids. In addition, a change in the total entropy generation is influenced by the angle of inclination of the magnet and the cylinder's rotational speed for Newtonian and dilatant fluids. Sasmal *et al.* [25] did numerical research on the laminar natural convection heat transfer in a power-law fluid from an isothermal rotating cylinder positioned coaxially in a square duct. The outcome showed that when the Rayleigh number and rotational velocity increase, the local Nusselt number distribution across the surface of the rotating cylinder progressively becomes uniform. Mahadi *et al.* [26] examined the issue of unsteady fourth-grade fluid flow within a rotating frame, considering the effects of magnetic fields and heat transfer. The analyses revealed that increasing magnetic and rotating parameters leads to decreased velocity, thereby reducing the motion. In an alternative presentation, many recent studies have investigated the influence of thermal performance in circular and other complicated enclosures alongside various factors, including magnetic fields, entropy generation, and nanofluids [27-35]. Saha *et al.* [27] focused their research on examining the impact of both the size and positioning of an obstruction on buoyancy-driven convection within a concentric annular configuration. Manna *et al.* [28] aimed to systematically assess the effects of heater and cooler positioning within four separate quadrantal cavities, each containing a hybrid nanofluid. These assessments were conducted under adiabatic conditions on the curved surface while subjecting the system to oriented magnetic fields. Chatterjee *et al.* [29] delved into characterizing magneto-hydrodynamics-driven thermal--fluid flow within cylinder-embedded annular thermal systems under conditions of peripheral differential heating. Chatterjee *et al.* [30] aimed to comprehend the positional influence of discrete heaters and coolers within a cylindrical thermal system undergoing a magneto-thermal convective process utilizing a hybrid nanofluid. Al-Srayyih *et al.* [31] explored the implications of introducing a pair of oscillating elliptical obstacles on natural convection and entropy generation within a quarter-circle cavity filled with a water-based hybrid nanofluid. Al-Amir

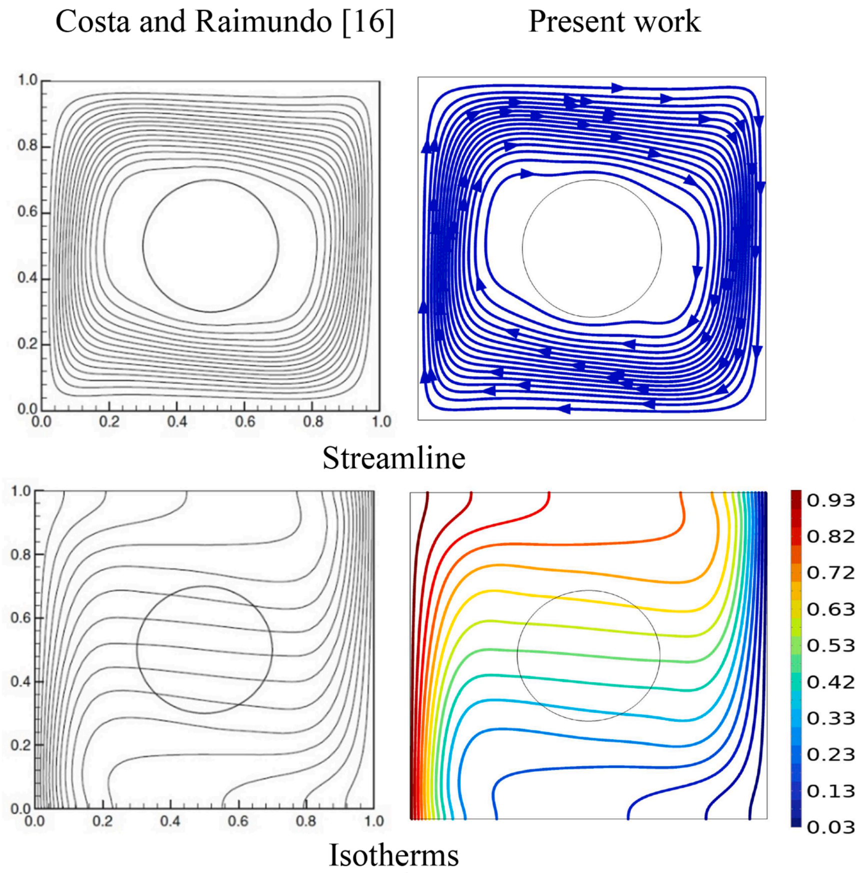

(a) $\omega^* = 0$

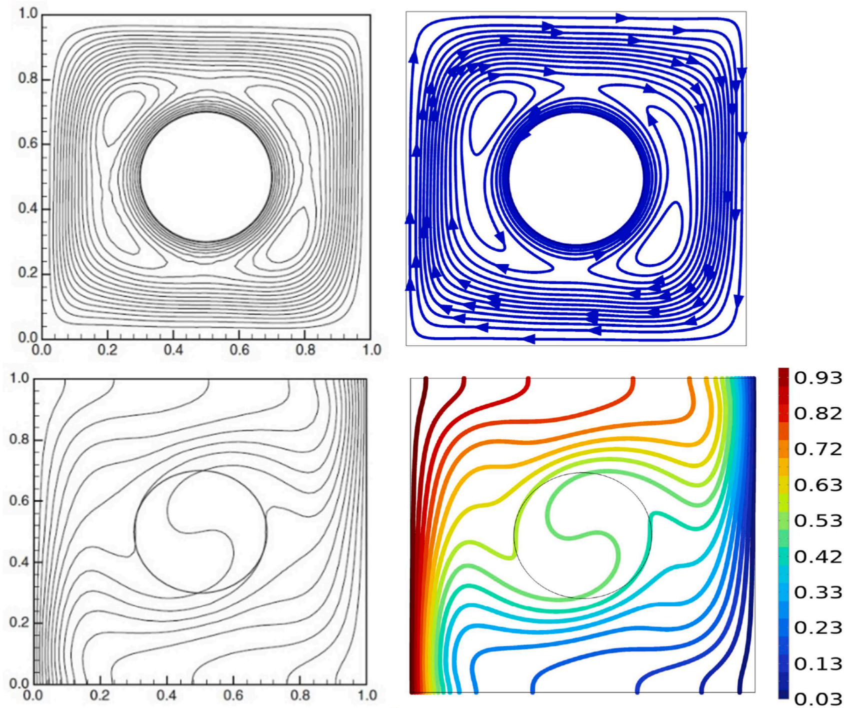

(b) $\omega^* = 500$

Fig. 4. Compression with Costa and Raimundo [16], at Ra = 10^5, $R_h = 1$, $R_{th.} = 1$, Pr = 0.6, $R^* = 0.2$ for (a) $\omega^* = 0$, (b) $\omega^* = 500$ and (c) $\omega^* = 500$.

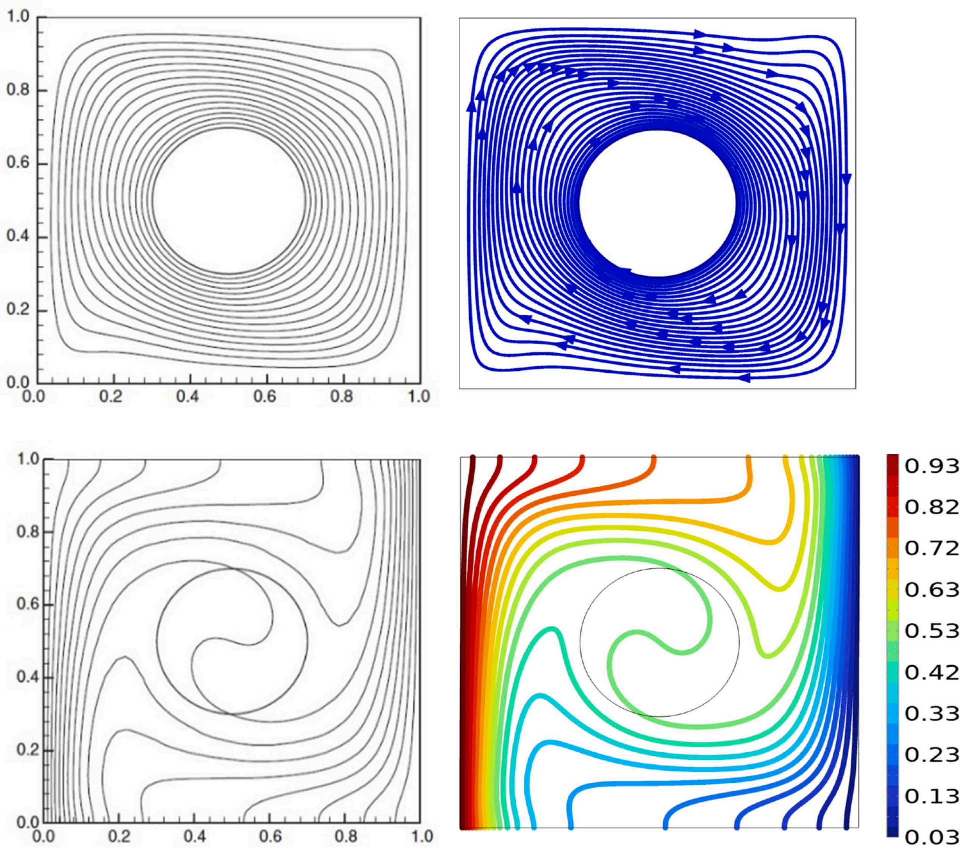

(c) $\omega^* = -500$

Fig. 4. (*continued*).

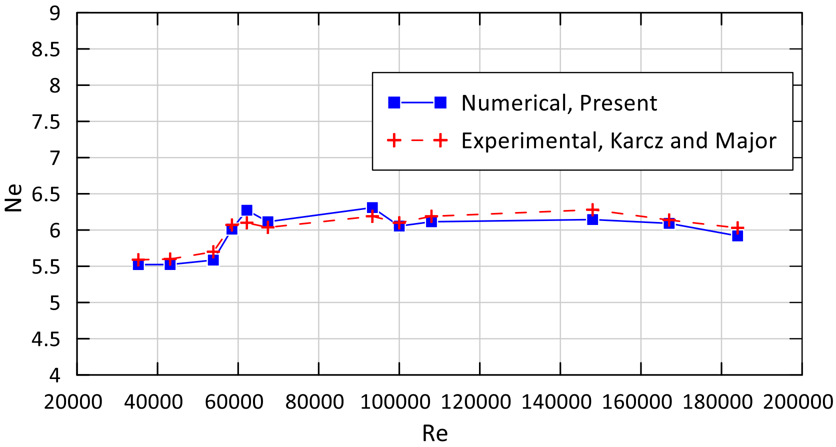

Fig. 5. Comparison of the numerical results from the present study with experimental results of Karcz and Major [37] involved calculating power consumption (Ne) across a range of Reynolds numbers.

Table 2
Varying geometrical parameters have been employed in this study.

	Ra	e*	r*	Nht	Nct
0 – 400	10^3 - 10^5	0.3 - 0.45	0.01 - 0.05	1 - 4	1 - 4

et al. [32] highlighted the importance of investigating natural convection within enclosures coupled with the depreciation of entropy generation, particularly in applications involving nanofluids and porous media, to enhance heat transfer efficiency, fluid flow dynamics, and overall system performance. Biswas *et al.* [33] examined the influence of wall curvature within a semicircular thermal annular system on magneto-nanofluidic flow, heat transfer, and entropy generation while maintaining constant cooling surface and fluid volume constraints. Al-Dulaimi *et al.* [34] emphasized the significance of improving the

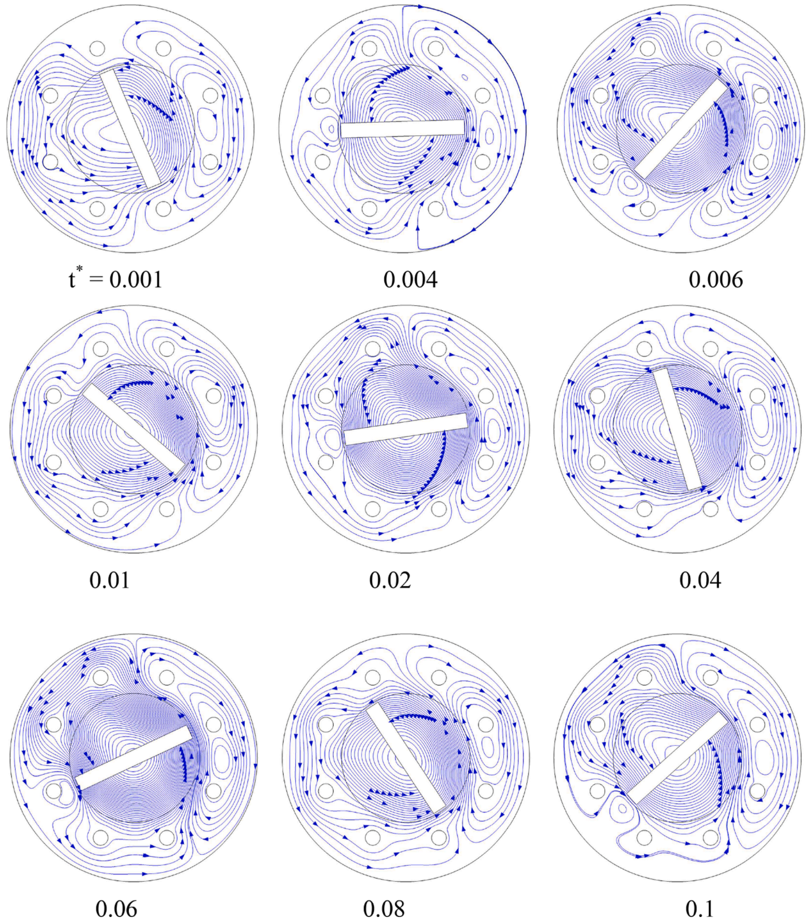

Fig. 6. (c) Progression of the Nusselt number with time at $r^* = 0.03$, $e^* = 0.35$, $Ra = 10^5$, $\omega^* = 400$ and Nht = 4, Nct = 4 located at $\varepsilon_2 = 45^\circ$ interval.

understanding of the effects of hybrid nanofluids on natural convection within complex enclosures for enhancing heat transfer efficiency. Akbar and Mustafa [35] noted that previous investigations into rotating flow often overlooked viscous heating effects, which arise from converting mechanical energy into heat due to friction.

Few researches focused on the experimental side of the rotation of the cylinder and the effect of heat transfer. Ozerdem and Toksoy [36] inspected experimentally the thermal convection between a rotating horizontal cylinder and the recirculation fluid in the cylinder. The results showed that the internal load coefficient increases the cylinder's rotation speed. They noted that the flow patterns in the rotating cylinder do not affect heat transfer. Karcz and Major [37] focused on the effect of baffle length on power consumption in an agitated vessel. Their experimental studies revealed that the power exhibited a significant dependence on the length of the baffle. Ma *et al.* [38] used a horizontal rotating cylinder surface to examine the concentration and temperature boundary layers. The findings showed that rotation has a distinct impact on the ascending side compared to the descending side. The concentration and temperature gradients on the ascending side developed steadily as the rotating Reynolds number increased. Salman *et al.* [39] studied experimentally the rotating cylinder at different speeds, as well as the angles of horizontal and vertical inclination were considered. The results showed that the heat transfer increases with the increase in speed and that the most significant value of the average Nusselt number occurs at an inclination angle of 90°.

A review of the existing literature reveals extensive studies on natural convection heat transfer across various geometries and internal obstacle shapes. Additionally, mixed convection heat transfer in enclosures with cylindrical objects has been a focal point in recent research. However, the rotation of non-circular objects remains relatively unexplored thoroughly. This gap could be attributed to the complexity of modeling such non-symmetrical objects' rotation, which often requires special treatment involving moving mesh techniques or a hybrid of rotating and fixed mesh approaches. Addressing this gap, the current study pioneers the modeling of a rectangular frame acting as an impeller inside a circular vessel comprising an array of cold and hot tubes. The novelty of this work, therefore, can be addressed by the use of a rotating-fixed frame methodology to capture the conjugate flow and heat transfer phenomena within the enclosure that houses the rotating rectangular obstacle. The modeling approach introduced in this study lays the foundation for simulating a wide range of real-world applications. Specifically, the geometry used in this research is particularly useful for optimizing systems like the simulation to various industrial applications such as biological reactors, chemical plants, and heat exchangers of nuclear reactors.

2. Mathematical formulation

The present configuration, depicted in Fig. 1, comprises a vessel of diameter D and a rectangular solid conductive cylinder. The rectangle frame length ($a = R$) and width ($b = 0.12$ R) are depicted in Fig. 1. The frame thermal conductivity ratio and heat capacity ratio are $R_{th.}$ and R_h, respectively. Here, the rotating rectangle is referred to as a rotating frame. The rotating frame rotates centrally with a counter-clockwise speed of ω. Bundles of tubes are distributed along a peripheral line adjusting to the vessel wall. Hot fluid flows through the tubes, bringing the tubes' surface temperature stable at T_h. The exterior surface of the vessel is thermally insulated. Water fills the vessel with $Pr = 6.9$. The no-

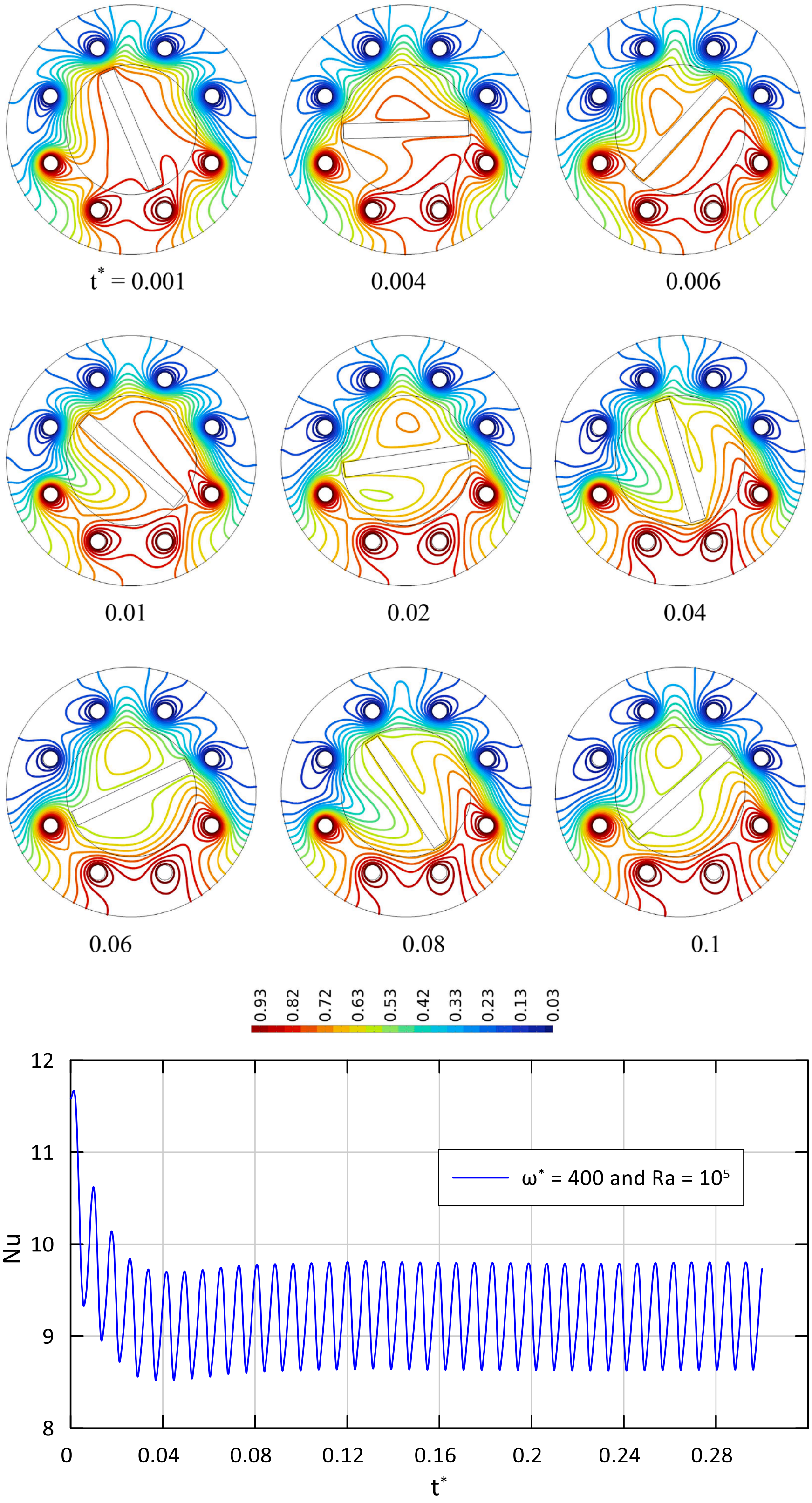

Fig. 6. (*continued*).

slip boundary is held on the solid boundaries. Considering the too-long dimension of the assembly, even the rotating impeller along the z-axis, the problem can be approximated to x-y 2D geometry. The density relates to temperature based on the Boussinesq approximation, which causes the buoyancy force.

The following relationship indicates the effective hydraulic diameter [40]:

$$D_h = 2 \times \frac{fluid\ volume}{wetted\ area} \tag{1-a}$$

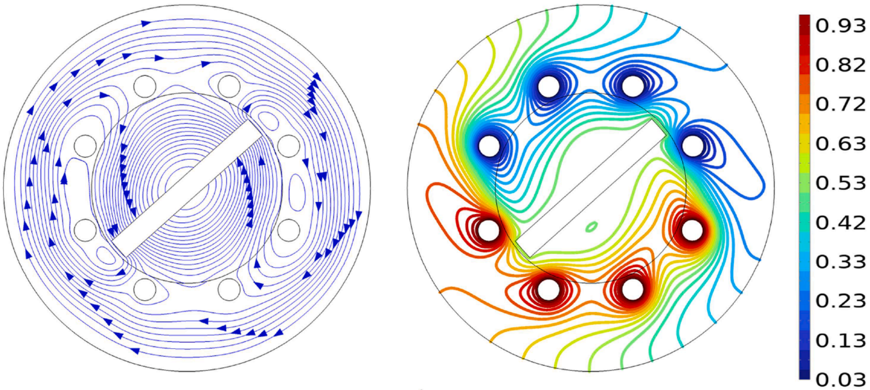

(a) $e^{*} = 0.3$

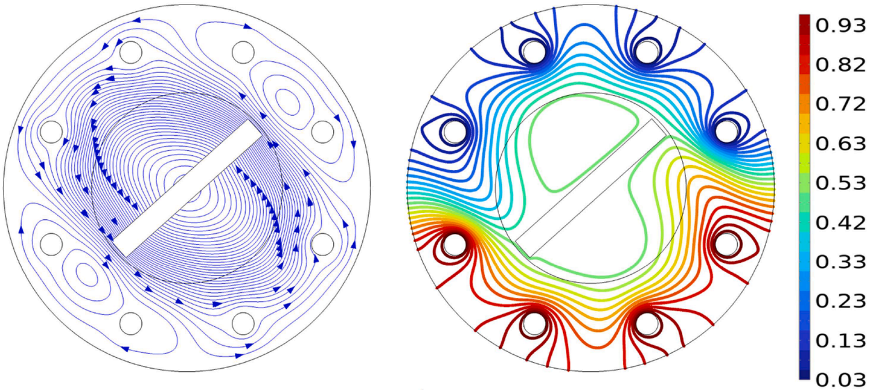

(b) $e^{*} = 0.4$

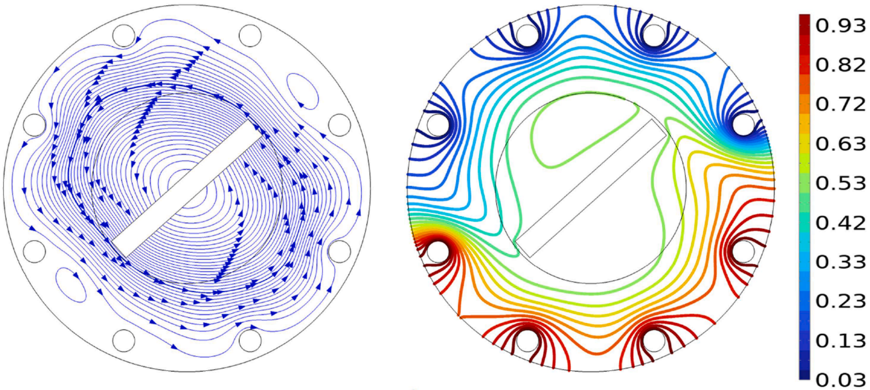

(c) $e^{*} = 0.45$

Fig. 7. Streamlines and isotherms for $Ra = 10^5$, $r^* = 0.03$, $Nht = Nct = 4$, $\varepsilon_2 = 45^\circ$, and $\omega^* = 400$ for (a) $e^* = 0.3$ (b) $e^* = 0.4$ and (c) $e^* = 0.45$.

$$D_h = 2\left(\frac{\pi R^2 - N\pi r^2 - ab}{2\pi R + 2N\pi r + 2(a+b)}\right) \tag{1-b}$$

where N is the number of hot and cold tubes.

The governing equations for unsteady-state, laminar, two-dimensional, incompressible flow with the Boussinesq approximation and constant fluid properties can be expressed in the global conservation equations describing the flow and thermal fields within a rotating frame as follows [41–43]:

$$\nabla.\overrightarrow{W} = 0 \tag{2}$$

$$\rho\frac{\partial\overrightarrow{V}}{\partial t} + \rho\nabla.\left(\overrightarrow{W}\otimes\overrightarrow{V}\right) + \rho\left(\overrightarrow{\omega}\times\overrightarrow{V}\right) = -\nabla p + \nabla.\left(\mu\nabla\overrightarrow{V}\right) + \overrightarrow{F}_b \tag{3}$$

$$\rho C_p\frac{\partial T}{\partial t} + \rho C_p\nabla.\left(\overrightarrow{W}\,T\right) = \nabla.(k\nabla\,T) \tag{4}$$

$$\left(\rho C_p\right)_s\frac{\partial T_s}{\partial t} = \nabla.(k_s\nabla\,T_s) \tag{5}$$

where $\overrightarrow{F}_b = \rho_0 g\beta(T - T_c)j$, and ω is the rotational velocity of the solid frame. Besides, $\overrightarrow{V} = \overrightarrow{W} + \overrightarrow{\omega}\times\overrightarrow{r}$ where $\overrightarrow{V}$ is the absolute velocity, $\overrightarrow{W}$ is the relative velocity, and $\overrightarrow{\omega}\times\overrightarrow{r}$ is the rotating frame velocity.

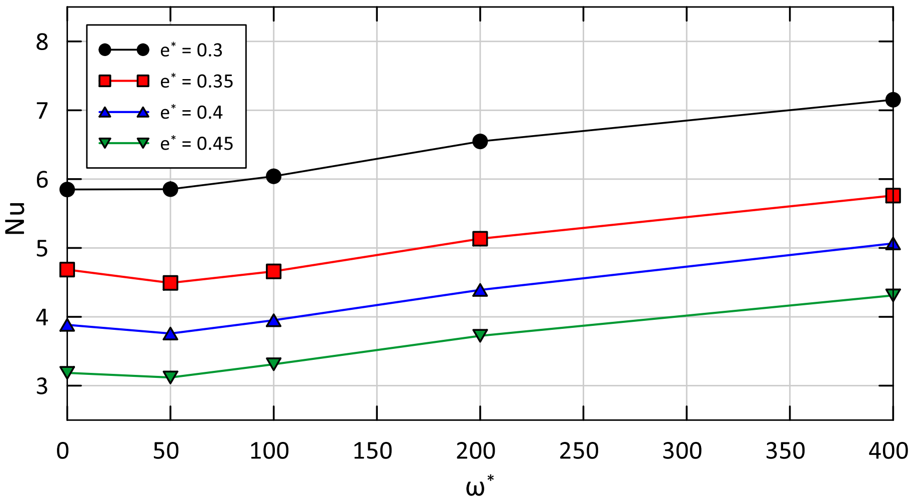

(a) Ra = 10^3

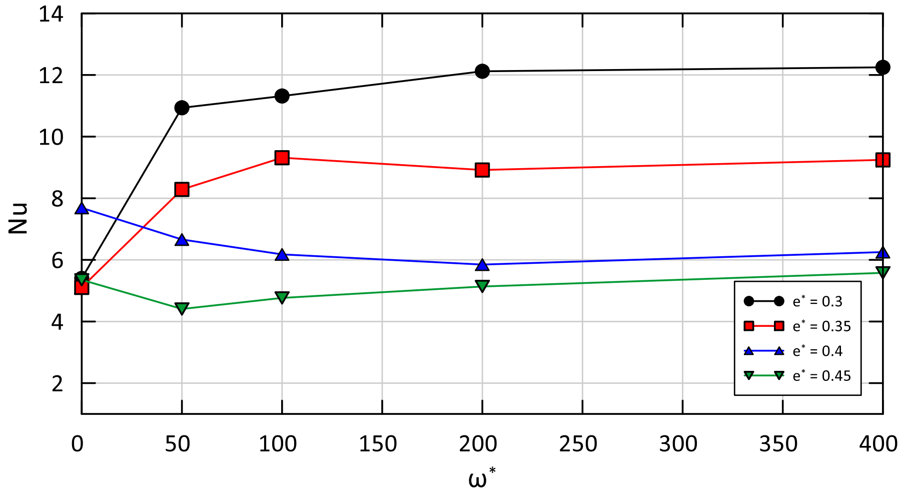

(b) Ra = 10^5

Fig. 8. Nusselt number distribution with the rotational speed for several radial positions of the hot tubes at (a) Ra = 10^3 and (b) Ra = 10^5.

Introducing the following non-dimensional parameters,

$$\nabla^* = \frac{\nabla}{D},\ e^*, r^* = \frac{e, r}{D}\ \theta = \frac{T - T_c}{T_h - T_c}, \omega^* = \frac{\omega\ D^2}{\alpha_f},\ \overrightarrow{V}^* = \frac{\overrightarrow{V}\ D}{\alpha_f},\ \overrightarrow{W}^* = \frac{\overrightarrow{W}\ D}{\alpha_f}, t^* = \frac{(\ t\ \alpha_f)}{D^2}, Ra = \frac{g\beta D_h^3 (T_h - T_c)}{\vartheta\ \alpha_f}, p^* = \frac{(p + \rho_0 g y)}{\left(\rho_f\ (\alpha_f / D)^2\right)}, Pr = \frac{\vartheta}{\alpha_f} \tag{6}$$

Because the hydraulic diameter varies with ranging the radius of the tubes r, we used the vessel diameter D instead of D_h in the parameters above.

The set of the conservation equations is remodeled as [40]:

$$\nabla^*.\overrightarrow{W}^* = 0 \tag{7}$$

$$\frac{\partial \overrightarrow{V}^*}{\partial t^*} + \nabla^*.\left(\overrightarrow{W}^* \otimes \overrightarrow{V}^*\right) + \left(\overrightarrow{\omega}^* \times \overrightarrow{V}^*\right) = -\nabla^* p^* + \mathrm{Pr}\nabla^{*2}\overrightarrow{V}^* + \overrightarrow{F}_b^* \tag{8}$$

$$\frac{\partial \theta}{\partial t^*} + \overrightarrow{W}^* \nabla^* \theta = \nabla^{*2}\theta \tag{9}$$

$$\frac{(\rho C_p)_s}{(\rho C_p)_f} \frac{\partial \theta_s}{\partial t^*} = \left(\frac{k_s}{k_f}\right) \nabla^{*2}\theta \tag{10}$$

where $\overrightarrow{F}_b^* = j\mathrm{RaPr}\theta$ and ω is the rotational speed of the solid frame.

The ratios R_h and $R_{th.}$ are identified as:

$$R_h = \frac{(\rho c_p)_s}{(\rho c_p)_f} \text{ and } R_{th.} = \frac{k_s}{k_f} \tag{11}$$

The dimensionless boundary conditions for the temperature walls of the enclosure are as follows:

$$\theta = 1 \text{ At the hot fluid through the tubes} \tag{12-a}$$

$$\theta = 0 \text{ At the cold fluid through the tubes} \tag{12-b}$$

$$\frac{\partial \theta}{\partial n} = 0 \text{ At the outer vessel wall (Isolated)} \tag{12-c}$$

$$\theta_s = \theta_f \text{The conditions along the periphery of the rotating frame} \tag{12-d}$$

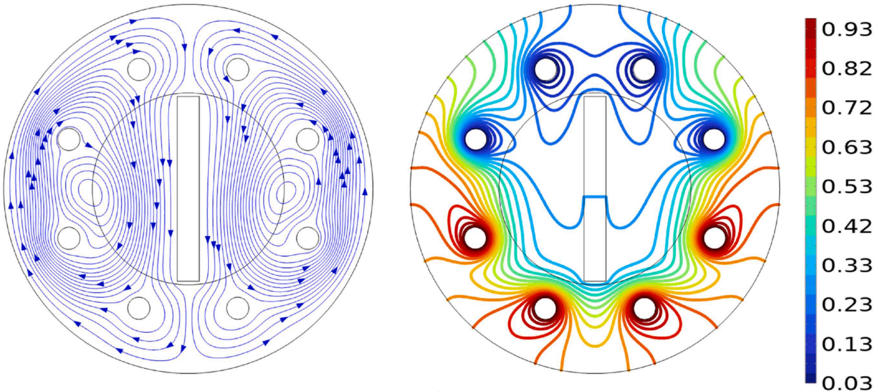

(a) $\omega^* = 0$

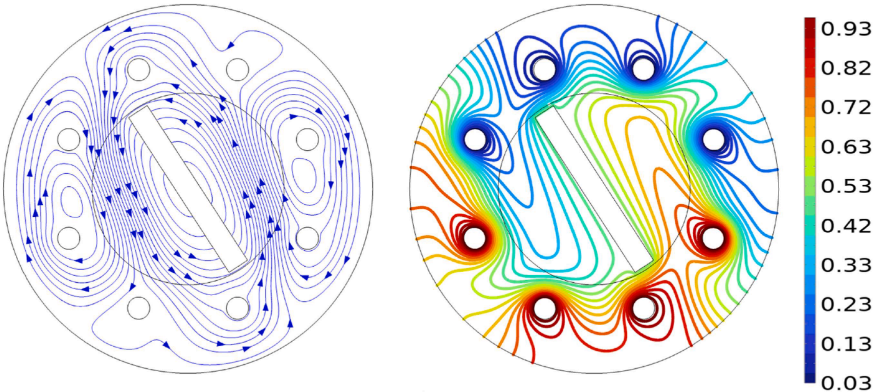

(b) $\omega^* = 100$

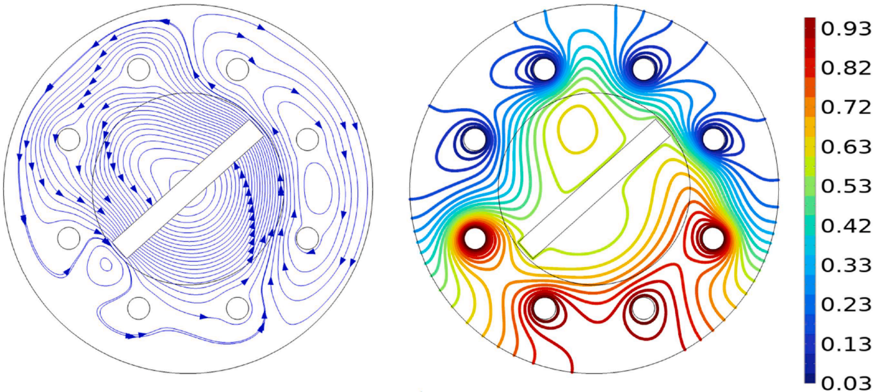

(c) $\omega^* = 400$

Fig. 9. Streamlines and isotherms for Ra = 10^5, r* = 0.03, e* = 0.35, Nht = 4, Nct = 4, ε_2 = 45° for rotational speed (a) ω* = 0, (b) ω* = 100, and (c) ω* = 400.

$$\left(\frac{\partial\theta}{\partial n}\right)_f = R_{th}\left(\frac{\partial\theta}{\partial n}\right)_s \tag{12-e}$$

The no-slip and impermeable boundary conditions are applied on all solid surfaces. The continuity of velocity and shear stress was applied at the fixed and rotating frame as well.

To estimate the dominant mode by which the heat is transferred, convection or conduction, Nusselt number along the walls of the hot tubes is adopted:

$$Nu = -\frac{1}{2\pi r}\int_0^{2\pi r}\left(\frac{\partial\theta}{\partial n}\right)dS \tag{13}$$

3. Numerical solution

The domain is divided into discrete elements, and the finite element method (FEM) is used to discretize equations (7) through (10). The finite element method uses the nonlinear residual equations that, in turn, are gotten from weighting the residuals (Galerkin equations). The governing equations are discretized over the entire domain except the hot and cold tubes. This method allows for accurate handling of both straight and curved borders. This method uses basis functions to define the unknown variables at each element's nodes. These basis functions interpolate the pressure, temperature, and velocity.

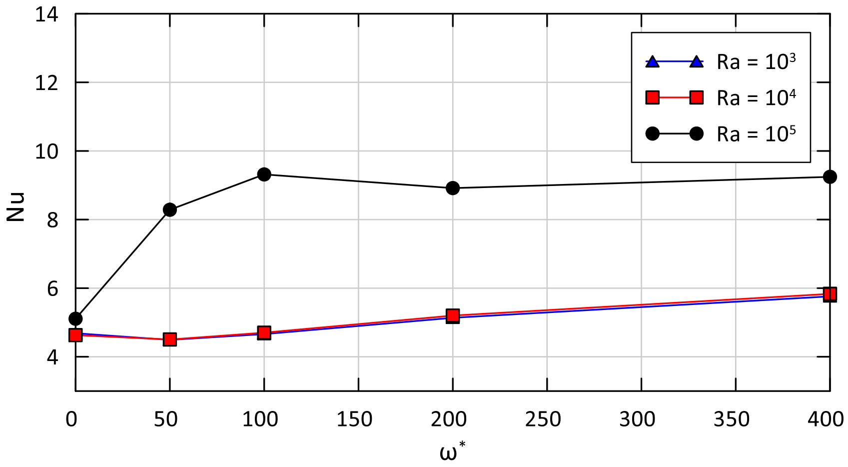

Fig. 10. Progression of the Nusselt number with the rotational speed for several Rayleigh numbers for $e^* = 0.35$, $r^* = 0.03$, Nht = 4, Nct = 4 and $\varepsilon_2 = 45^\circ$.

the the $$u^*, v^* \approx \sum_i^M (u^*, v^*)_i^k \Phi_i^k(x^*, y^*), \quad \theta \approx \sum_i^M \theta_i^k \Phi_i^k(x^*, y^*), \; p^* \approx \sum_i^M p^{*k}_i \Phi_i^k(x^*, y^*) \tag{14}$$

where i represents the node number, k represents the time iteration, and M represents the number of nodes.

Specifically, a weak form of the governing equations was integrated across mesh elements to derive residual equations, which were subsequently solved using a second-order algorithm. The solution of these equations was facilitated by the Parallel Direct Solver (PARDISO) [44–48]. PARDISO is designed to efficiently handle large sparse linear systems of equations by leveraging parallel processing, thereby significantly reducing computation time. Additionally, the coupled equations were tackled using the Newton method with a damping factor of 0.80 and a relative error criterion of less than 10^{-3} to ensure accuracy. To enhance stability, second-order upwind and crosswind stabilization schemes were implemented, effectively mitigating numerical instabilities arising from convective and diffusive terms. The step of the time is taken as 0.001. The illustration depicted in Fig. 2 delineates the procedural outline of the FEM, showcasing the numerical processes involved.

The percentage error for two successful computation is up to 5×10^{-3}, according to the

$$\left|\frac{\left|\Gamma^{j+1} - \Gamma^{j}\right|}{\Gamma^{j+1}}\right| \leq 5 \times 10^{-3} \tag{15}$$

j refers to the iteration number and Γ may be pressure, temperature or velocity. In the numerical analysis, after substituting the equations, two main operations occur, the first of which is the selection of the appropriate mesh, and the domain is firstly subdivided using an automatic mesh generating algorithm. The second is for comparison with the results of other researchers to obtain accuracy, as shown below in detail:

3.1. Grid refinement check

The Nusselt number, streamlines, and isotherms are considered to check the convergence state of a vessel containing four hot tubes and four cold tubes, each with radius $r^* = 0.03$, and those tubes had their centers far from the center of the vessel at $e^* = 0.35$ with the Rayleigh number of 10^3 and several angular rotations $\omega^* = 0 - 400$. Four hot tubes arranged at angles $\varepsilon_1 = 22.5^\circ, 67.5^\circ, 112.5^\circ$ and 157.5° and four cold tubes arranged at an angle $\varepsilon_1 = 202.5^\circ, 247.5^\circ, 292.5^\circ$ and 337.5° with $\varepsilon_2 = 45^\circ$ interval. The tested mesh sizes (shown in Fig. 3(a)) helped us to adopt the size of 174,080 elements (portrayed in Fig. 3(b)) based on the accuracy and the time expended in the calculations.

3.2. Verification of results

To verify the accuracy of the numerical scheme and to obtain the best results, a test was performed with Costa and Raimundo [16], represented by a mixed convection inside a square enclosure. One side is exposed to heat, the opposite wall is cold, and the rest are thermally insulated. A circular cylinder in the middle rotates clockwise and counterclockwise. Costa and Raimundo adopted a rotating cylinder as the rotating geometry. Since the cylinder geometry is symmetric, using a fixed frame approach was possible in [16]. In the present study, we introduced the rotating cylinder approach, which can solve the models with no-symmetric shapes such as rectangular cylinders. We simulated the same rotating cylinder heat transfer in an enclosure [16] using the new proposed rotating frame approach.

The Prandtl number is fixed at 0.6 (air), and the Rayleigh number is 10^5. The mean Nusselt number was calculated for several speeds, and the percentage error was calculated during the comparison. This comparison gave excellent results, as shown in Table 1. In addition, the isotherms and the streamlines contours were drawn, demonstrating consistent patterns, as shown in Figs. 4 (a-c).

Additional validation with experimental results was conducted to ascertain the accuracy of the present scheme. The experiments were conducted by Karcz and Major [37] within an agitated vessel with an inner diameter of 0.6 m, filled with tap water. A Rushton turbine with a diameter of 0.198 m was positioned at a height of 0.198 m from the vessel bottom. The study focused on the turbulent fluid flow regime within the vessel, specifically targeting Reynolds numbers ranging from 3×10^4 to 2×10^5. The dimensionless equations of the present study were adapted along with the kinetic energy and dissipation equations (κ-ϵ) equations to calculate the power consumption as a function of Reynolds numbers. Fig. 5 illustrates highly favorable outcomes, enhancing confidence in the accuracy of the current numerical approach.

4. Results and discussion

To accommodate the present problem, dimensionless pertinent parameters are set as follows. The fluid is water with a Prandtl number of Pr = 6.9; the values of the Rayleigh numbers are 10^3,10^4 and 10^5, while the angular rotational speed is taken as 0, 50, 100, 200, and 400, respectively. The thermal conductivity ratio of the frame to fluid $R_{th.}$ and the heat capacity ratio R_h are fixed at 397.63 and 0.582, respectively. The results are gathered into four sets of geometrical parameters: the first focuses on the radial position (e^*), the second offers the impact of

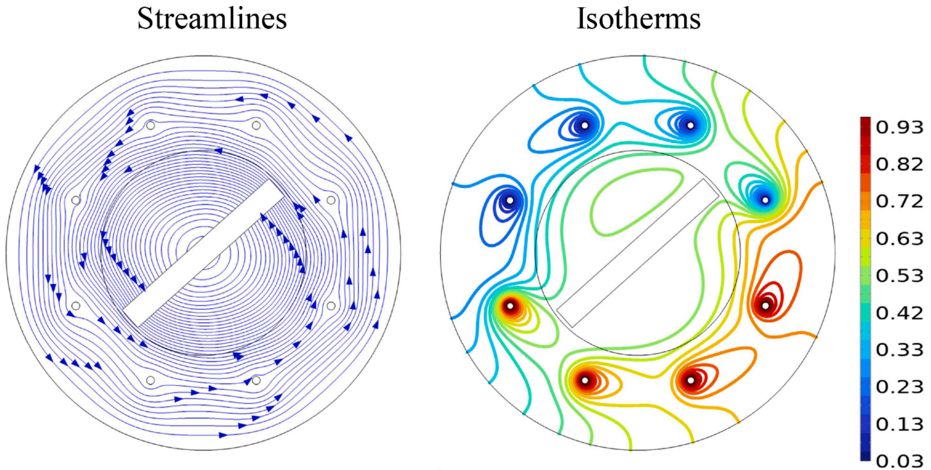

(a) $r^* = 0.01$

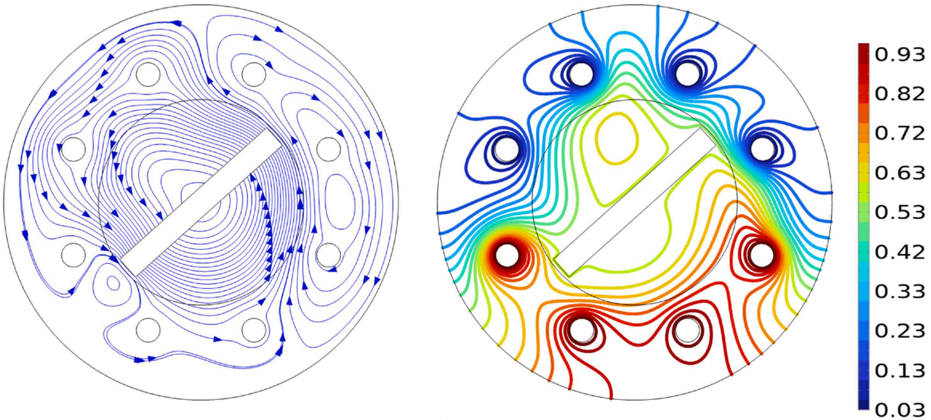

(b) $r^* = 0.03$

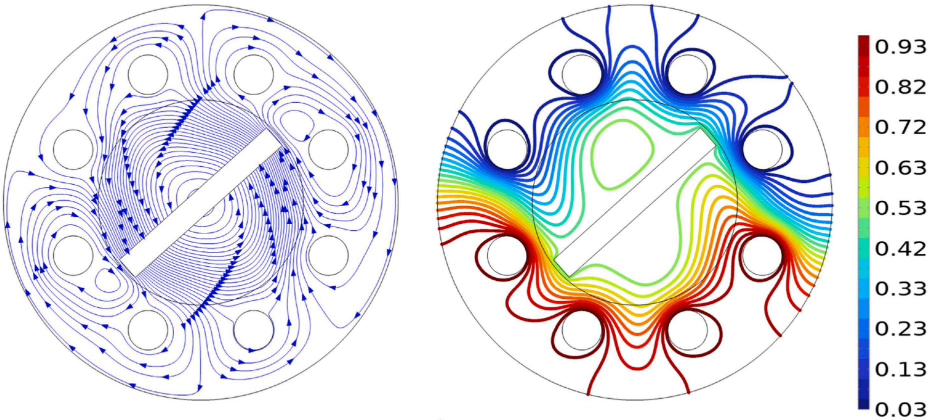

(c) $r^* = 0.05$

Fig. 11. Streamlines and isotherms at Ra = 10^5 $\omega^* = 400$, $e^* = 0.35$, Nht = Nct = 4, and $\varepsilon_2 = 45^\circ$ for (a) $r^* = 0.01$, (b) $r^* = 0.03$ and (c) $r^* = 0.05$.

the rotational speed of the impeller (ω^*), the third focuses on the size of the hot tubes (r^*), while the last focused on the number of these tubes in the vessel (N). The results in each set were studied in detail, the contours of the flow and isotherms were portrayed, and the mode of the heat transfer was studied by calculating the Nusselt number. In this study, the radial position (e^*), size (r^*), and number (Nht) of the hot tubes positioned in the upper part of the vessel are regulated according to identical parameters as those specified for the cold tubes situated on the opposing side, in the lower part of the vessel. The ranges of the studied parameters are illustrated in Table 2.

It is interesting, at first, to test the cyclic patterns of the streamlines and the isotherms and to examine how long they take to reach the cyclic steady state. The following subsection discovers this behavior

4.1. Cyclic steady state

The contours shown in Figs. 6(a) and (b) display the streamlines and isotherms to show the transient behaviors. Four hot tubes arranged at the upper half of the vessel at angles $\varepsilon_1 = 22.5^\circ, 67.5^\circ, 112.5^\circ$ and 157.5° and four cold tubes placed at the lower half of the vessel at angles $\varepsilon_1 =$

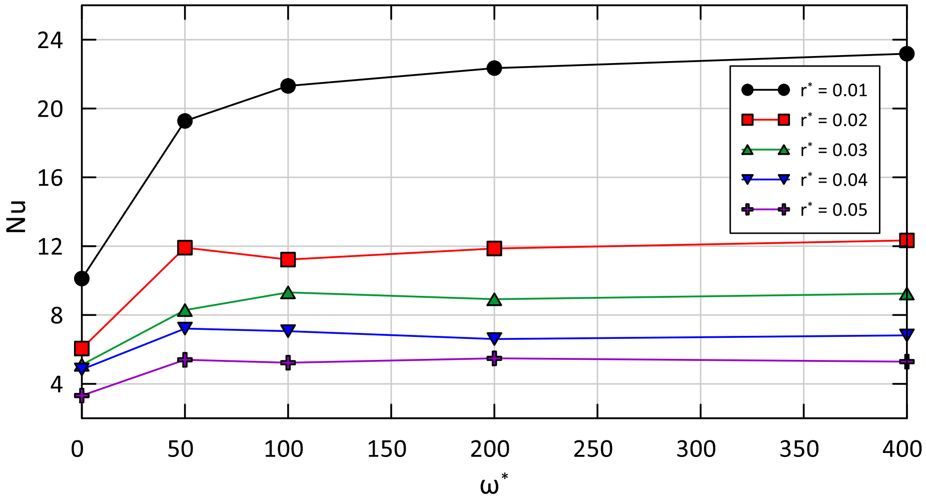

Fig. 12. shows the Progression of the Nusselt number for Ra = 105 with the rotational speed and several tube radii r* for e* = 0.3, Ra = 105, Nht = Nct = 4, and ε_2 = 45° interval.

202.5°, 247.5°, 292.5° and 337.5° with $\varepsilon_2 = 45°$ interval. All tubes are fixed at a radius r* = 0.03 for each, and those tubes have their centers far from the vessel's center at e* = 0.35. The Rayleigh number was taken as 10^5 and the angular velocity at 400. The time step was taken at 0.001 to obtain a faster resolution time and to explain the movement of the frame and the progression of the streamlines more accurately.

For an early time, t* = 0.001, the fluid movement and eddies begin to form inside the vessel where the buoyancy force is dominant, which interacts obviously with the fluid motion. With time progressing, the counterclockwise rotation of the frame reacts with the rising buoyant fluid, leading to the following actions. (i) In the left part of the vessel, the rotating frame impedes the rising buoyancy force while it assists those rising in the right half of the vessel. (ii) Thereby, a clockwise rotating thorough eddy encompasses tubes in the right half of the vessel. Beyond about t* = 0.04, the streamlines are irrespective of time, indicating the steady state mixed convection.

Within the first evolution stages, the interaction between the buoyancy force and the rotating impeller is weak; thus, the isotherms (Fig. 6 (b)) are arranged around each tube with a skewed plume. The skewness of the hot plumes pursues the trace of the rotating impeller. As the streamlines develop with time, the hot plumes of the lower tubes follow the direction of the frame rotation. Generally, for non-horizontal frame position, the adjacent isotherms look stratified.

The time augmentation of the Nusselt number depicted in Fig. 6(c) endorses the early stabilization of the heat exchange inside the vessel-rotating impeller assembly. Almost, at t* = 0.04, the average Nusselt number reaches its steady value.

4.2. *The impact of the tube's radial position*

Studying the role of the distance of hot tubes from the cold pipes, e*, by the streamlines and isotherms is highlighted in this section. The other parameters are fixed at Nht = Nct = 4, r* = 0.03, Ra = $10^{5,}$ and various speeds were taken from 0 to 400. Fig. 7 exemplifies three maps of isotherms and streamlines for three values of the tube's radial position. It is worth mentioning that e* is measured from the center of the vessel to the center of the tubes. For the lower value of the radial position (e* = 0.3), the proximity of the tubes to the rotating frame leads to disturbed and asymmetric streamlines around the tubes, which in turn produces a notable hot and cold plume of isotherms as shown in Fig. 7(a). Moreover, drifting the tubes from the adiabatic vessel provides a free region for fluid to convey the gradient of temperature. Increasing the radial distance to e* = 0.4 (Fig. 7(b)) and 0.45 (Fig. 7(c)) keeps the tubes away from the rotating frame and brings them next to the adiabatic wall. This distance attenuates the action of the rotating frame and hence generates a symmetry of streamlines about the exes of the rotating frame. In this case, heat exchange occurs primarily due to natural convection. This deduction is drawn from the uniform and symmetric isotherms, irrespective of the rotating frame.

To evaluate the role of the tube radial position, e*, on the development of the heat transfer, the Nusselt number is plotted in Figs. 8(a) and (b) for a given Rayleigh number and several rotational speeds. Obviously, the lower the e* value, the greater the Nusselt number, which is due to two reasons. The first is the proximity of hot tubes to the cold tubes, which decreases the thermal resistance of heat transfer. The second reason is the proximity of the frame edges to the hot surface, which enables an active mixing process. For ω* = 200, as the radial distance is reduced from 0.45 to 0.3, the Nusselt number elevates to 75.83 % and 135.95 % for Ra = 10^3 and 10^5, respectively. Overall, it is also noticed that the Nusselt number elevates with the rising rotational speed due to the role of mixing resulting from the movement of the fluid, which stimulates the role of forced convection.

4.3. *The impact of the rotational speed*

In addition to the implication of the impact of the rotational speed in the previous section, it is opportune to explain this impact separately in this section. For e* = 0.35, the stationary frame demonstrates the pure natural convection with symmetric streamlines about the vertical y-axis with convection cells circulating in a counter manner, as shown in Fig. 9 (a). This circulation results in symmetric isotherms about the y-axis with dense thermal boundary layers around the lower hot tubes. As ω* = 100, Fig. 9(b) reveals two counter-rotating vortices, each confining two differentially heated tubes. This contributes to efficient mixing and heat exchange, which can be identified by the thermal stratification along the sides of the rotating frame and the distinct plumes extending from the tubes.

With stronger rotation (ω* = 400, Fig. 9(c)), the momentum delivered to the fluid escalates, attenuating the plumes of the isotherms, and the left circulation encloses two cold tubes that reduce the benefit of the heat exchange. This effect is clearly explained by the Nusselt number distribution of Fig. 10, where at Ra = 10^5, the speed of ω* = 100 demonstrates a maximum Nusselt number. For a relatively low Rayleigh number, this scenario is not observed because the heat exchange is mainly due to the rotational mixing rather than the buoyancy effect. Generally, as the rotational speed is raised from zero to 200, the Nusselt number is augmented by 9.57 % and 74.59 % for Ra = 10^3 and 10^5, respectively. The reader may wonder why the rotational speed is more

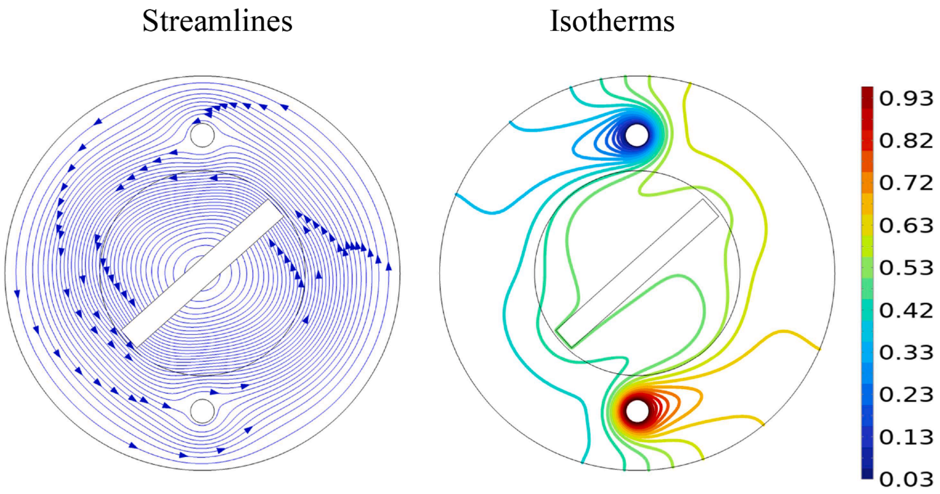

(a) Nht = 1

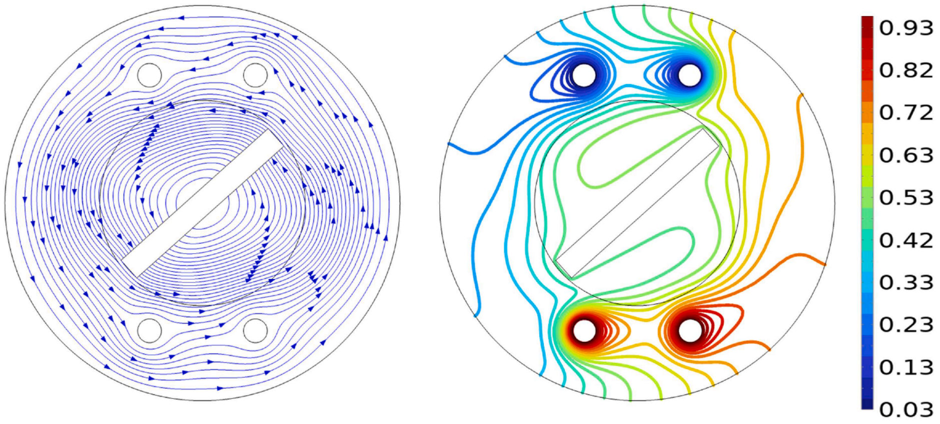

(b) Nht = 2

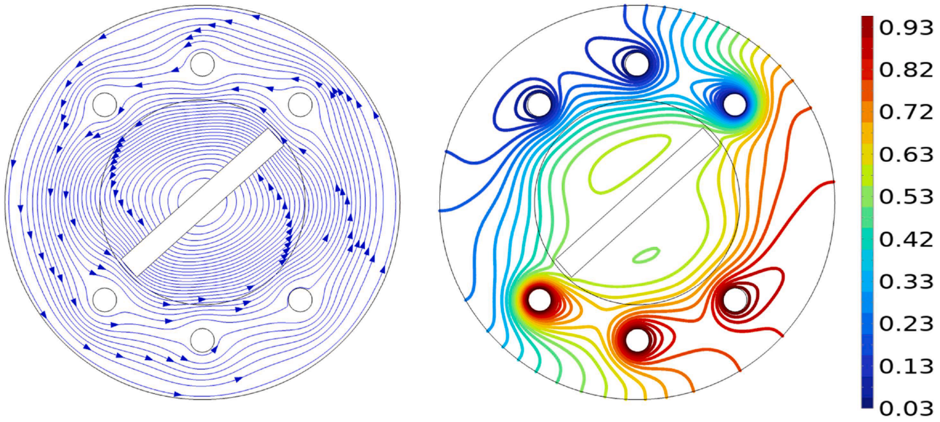

(c) Nht = 3

Fig. 13. Streamlines and isotherms for Ra = 10^5, e* = 0.35, r* = 0.03, ω* = 400 for (a) Nht = 1, (b) Nht = 2 and (c) Nht = 3.

effective in the higher Rayleigh number. We answer as follows: in the higher Rayleigh number, the buoyancy force is relatively strong. Thus, the fluid motivated by the rotating frame drives the heat with less confusion.

4.4. *Effect of the size of the tubes*

The size of the tubes and their effect are inspected at Ra = 10^5, e* = 0.35, Nht = Nct = 4, and ω* = 400, as depicted in Fig. 11. The streamlines of Fig. 11(a) imply that as the size of the tubes is small enough (r* = 0.01), a little drag encounters the circulated fluid. Therefore, the streamlines are so uniform and symmetric leading to

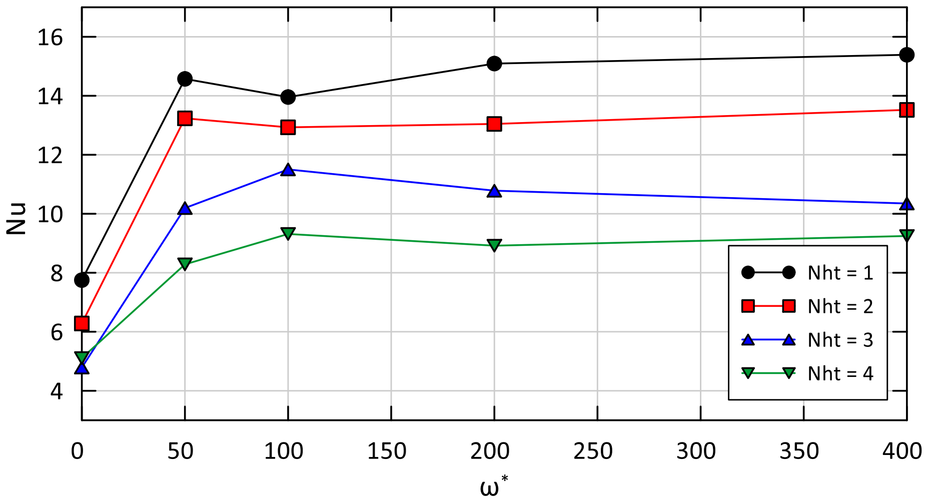

Fig. 14. Nusselt number variation for several numbers of tubes with at e* = 0.35, r* = 0.03, and Ra = 10^5.

sequential cold and hot plumes in the isotherms. As the tube size is enlarged to r* = 0.03 (Fig. 11(b)), the fluid separates from the tubes surfaces resulting in wake zones. It is well-known that the wake zones grow with the size of the bluff body (tube) and the fluid velocity, causing weak energy exchange.

Based on the tube position and the frame rotation, the wake zones interact randomly with buoyancy force, leading to random plumes and disturbing the symmetry of the streamlines. This context is seen clearly when the radius is raised to r* = 0.05, as displayed in Fig. 11(c). The Nusselt number progression with the size of the tubes is presented in Fig. 12, where the rotational speed is also depicted in this category. The figure displays a uniform elevation in the Nusselt number with decreasing the tube size, where the percentage increase of the Nusselt number at ω* = 200 and Ra = 10^5 is about 308 % when the tube size reduces from 0.05 to 0.01. This is mainly due to the emergence of uniform streamlines at smaller tube radii. Fig. 12 also exemplifies that the rotational speed beyond ω* = 200 becomes useless. This effect is explained by the drag and separation impeding the heat exchange at high rotational speeds.

4.5. *Varying the number of tubes*

This section investigates the role of the rotational speed with various hot and cold tubes. The Rayleigh number is fixed at 10^5, the distance of the hot tubes from the center at e* = 0.35, and the radius of the tubes is set at r* = 0.03. Fig. 13 displays one main recirculation inside the vessel for all combinations of the tubes. This tendency is well expected due to the low obstacle effect emerging with a relatively small tube size (r* = 0.03), introducing slight deceleration to the rotating fluid. The isotherms show skewed hot and cold plumes following the direction of the rotating frame.

Fig. 14 portrays similar trends of the Nusselt number with rotational speed for different numbers of tubes. This demonstrates that the role of the rotational speed is held regardless of the number of hot and cold tubes. On the other hand, the decline of the average Nusselt number with elevating the number of tubes can be exemplified by the intensifying of the temperature gradient around the hot singular tube. Increasing the tubes mitigates the intensification of the temperature gradient. Thus, the Nusselt number averaged along a peripheral of the hot tube(s) is higher with fewer tubes. The percentage increases in the Nusselt numbers at ω* = 200 as follows (20.91 %, 46.29 %, and 69.23 %) when the number of tubes is reduced from (4 to 3 tubes), (4 to 2 tubes) and (4 to one tube) respectively.

5. Conclusions

Heat exchange between cold and hot tubes inside a vessel is augmented using a rotating frame. This problem is investigated numerically in this paper. The rotational speed, size, location, and number of the tubes and the Rayleigh number were parameterized to perform the study. The study finds that the radial position, rotational speed, size, and the number of tubes significantly influence heat transfer in the system and should be considered in the design of vessel and tube heat exchangers. The main outcomes can be summarized as follows:

- The heat transfer is augmented when the radial position of the tubes becomes closer to the rotating frame. For example, displacing the tubes from the vessel wall towards the rotating frame (by reducing the radial position from e* = 0.45 to 0.3 raises the Nusselt number by 75.83 % at Ra = 10^3 and 135.95 % for Ra = 10^3.
- The frame speed augments the Nusselt number, while it becomes useless when it exceeds the critical value of ω* = 200 because of the drag and flow separation around the tubes. It is recorded that Nusselt number rises by 74.59 % and 9.57 % for Ra = 10^5 and 10^3, respectively, as the rotational speed (ω*) is raised from 0 to 200 for e* = 0.35.
- Because of the drag effect and the temperature concentration, the smaller the tube size, the greater the Nusselt number. The Nusselt number elevates by 308 % when the tube size is reduced from r* = 0.05 to r* = 0.01 at ω* = 200.
- The Nusselt number elevates monotonically as the number of heat-exchanging tubes decreases. This behavior is exemplified by the intensifying of the temperature gradient around a single tube. Specifically, the percentage increase of the Nusselt numbers at ω* = 200 is 20.91 %, 46.29 %, and 69.23 % when the number of tubes is reduced from 4 to 3 tubes, 4 to 2 tubes, and 4 to one tube, respectively.
- The role of the rotational speed of the frame showcases the same trend for different numbers of tubs.
- The recommended best parameter range is as follows: tube radius r* = 0.01, tube position e* = 0.3, rotational speed ω* = 200, and Rayleigh number Ra = 10^5. This recommendation is based on the higher Nusselt number with lower rotational speed (to save power consumption).

In general, this numerical study demonstrates that the radial position, rotational speed, and the size of the hot tubes in the vessel significantly influence the exchange of heat in the system. These factors should be carefully considered when designing the mixer. It is demonstrated that mixing and rotation of the frame play crucial roles in enhancing heat transfer. Consequently, future studies can focus on using flexible baffles to get better benefits from the rotating frame.

CRediT authorship contribution statement

Ali Q. Abd Al-Hasan: Writing – original draft, Visualization, Validation, Software, Investigation, Data curation. **Muneer A. Ismael:** Writing – review & editing, Visualization, Supervision, Methodology, Conceptualization. **Mohammad Ghalambaz:** Writing – review & editing, Supervision, Methodology, Investigation, Formal analysis, Conceptualization.

Declaration of competing interest

The authors declare that they have no known competing financial interests or personal relationships that could have appeared to influence the work reported in this paper.

Data availability

Data will be made available on request.

References

[1] E. Dominguez-Ontiveros, Y.A. Hassan, Experimental study of a simplified 3× 3 rod bundle using DPTV, Nuclear Eng. Design 279 (2014) 50–59.
[2] R. Azzouz, M.B.B. Hamida, Natural convection in a circular enclosure with four cylinders under magnetic field: application to heat exchanger, Processes 11 (2023) 2444.
[3] M.H. Machi, I. Farkas, J. Buzas, Enhancing solar air collector performance through optimized entrance flue design: a comparative study, Internat. J. Thermofluids 21 (2024) 100561.
[4] P. Zhang, X. Zhang, J. Deng, L. Song, A numerical study of natural convection in an inclined square enclosure with an elliptic cylinder using variational multiscale element free Galerkin method, Int. J. Heat. Mass Transf. 99 (2016) 721–737.
[5] B. Karbasifar, M. Akbari, D. Toghraie, Mixed convection of Water-Aluminum oxide nanofluid in an inclined lid-driven cavity containing a hot elliptical centric cylinder, Int. J. Heat. Mass Transf. 116 (2018) 1237–1249.
[6] Y.M. Seo, M.Y. Ha, Y.G. Park, A numerical study on the three-dimensional natural convection with a cylinder in a long rectangular enclosure. Part I: size effect of a circular cylinder or an elliptical cylinder, Int. J. Heat. Mass Transf. 134 (2019) 420–436.
[7] Y.G. Park, M.Y. Ha, C. Choi, J. Park, Natural convection in a square enclosure with two inner circular cylinders positioned at different vertical locations, Int. J. Heat. Mass Transf. 77 (2014) 501–518.
[8] N. Ghaddar, F. Thiele, Natural convection over a rotating cylindrical heat source in a rectangular enclosure, Numerical Heat Transfer 26 (6) (1994) 701–717.
[9] N. Ghaddar, Natural convection over rotating cylindrical heat source in an enclosure, J. Thermophys. Heat. Trans. 10 (2) (1996) 303–311.
[10] R.E. Morales, A. Balparda, A. Silveira-Neto, Large-eddy simulation of the combined convection around a heated rotating cylinder, Int. J. Heat. Mass Transf. 42 (5) (1999) 941–949.
[11] M.S. Sadeghipour, Y.P. Razi, Natural convection from a confined horizontal cylinder: the optimum distance between the confining walls, Int. J. Heat. Mass Transf. 44 (2) (2001) 367–374.
[12] Y. Yan, Y. Zu, Numerical simulation of heat transfer and fluid flow past a rotating isothermal cylinder–a LBM approach, Int. J. Heat. Mass Transf. 51 (9–10) (2008) 2519–2536.
[13] P.J. Singh, S. Roy, I. Pop, Unsteady mixed convection from a rotating vertical slender cylinder in an axial flow, Int. J. Heat. Mass Transf. 51 (5–6) (2008) 1423–1430.
[14] J. Ghazanfarian, M. Nobari, A numerical study of convective heat transfer from a rotating cylinder with cross-flow oscillation, Int. J. Heat. Mass Transf. 52 (23–24) (2009) 5402–5411.
[15] S.B. Paramane, A. Sharma, Heat and fluid flow across a rotating cylinder dissipating uniform heat flux in 2D laminar flow regime, Int. J. Heat. Mass Transf. 53 (21–22) (2010) 4672–4683.
[16] V. Costa, A. Raimundo, Steady mixed convection in a differentially heated square enclosure with an active rotating circular cylinder, Int. J. Heat. Mass Transf. 53 (5–6) (2010) 1208–1219.
[17] S.H. Hussain, A.K. Hussein, Mixed convection heat transfer in a differentially heated square enclosure with a conductive rotating circular cylinder at different vertical locations, Internat. Communicat. Heat Mass Transfer 38 (2) (2011) 263–274.
[18] C.C. Liao, C.A. Lin, Mixed convection of a heated rotating cylinder in a square enclosure, Int. J. Heat. Mass Transf. 72 (2014) 9–22.
[19] T. Wang, Z. Huang, G. Xi, Entropy generation for mixed convection in a square cavity containing a rotating circular cylinder using a local radial basis function method, Int. J. Heat. Mass Transf. 106 (2017) 1063–1073.
[20] K. Khanafer, S. Aithal, Mixed convection heat transfer in a lid-driven cavity with a rotating circular cylinder, Internat. Communicat. Heat Mass Transfer 86 (2017) 131–142.
[21] K. Luo, J. Wu, H.L. Yi, H.P. Tan, Numerical investigation of heat transfer enhancement in electro-thermo-convection in a square enclosure with an inner circular cylinder, Int. J. Heat. Mass Transf. 113 (2017) 1070–1085.
[22] T. Wang, Z. Wang, G. Xi, Z. Huang, Periodic unsteady mixed convection in square enclosure induced by inner rotating circular cylinder with time-periodic pulsating temperature, Int. J. Heat. Mass Transf. 111 (2017) 1250–1259.
[23] M.A. Ismael, O. Younes, M. Fteiti, M. Ghalambaz, R.Z. Homod, Impingement jets on a confined assembly of rotating hot cylinder covered by a surface porous layer, Appl. Therm. Eng. 229 (2023) 120470.
[24] F. Selimefendigil, H.F. Öztop, MHD mixed convection and entropy generation of power law fluids in a cavity with a partial heater under the effect of a rotating cylinder, Int. J. Heat. Mass Transf. 98 (2016) 40–51.
[25] C. Sasmal, A. Gupta, R. Chhabra, Natural convection heat transfer in a power-law fluid from a heated rotating cylinder in a square duct, Int. J. Heat. Mass Transf. 129 (2019) 975–996.
[26] S. Mahadi, Y.S. Hoe, N. Arbin, F.S.M. Nasrudin, Hybrid numerical approach for MHD fourth-grade non-Newtonian fluid flow in a rotating frame over semi-infinite boundary condition with a presence of heat transfer, in: AIP Conference Proceedings, AIP Publishing, 2024.
[27] A. Saha, A. Chakravarty, K. Ghosh, N. Biswas, N.K. Manna, Role of obstructing block on enhanced heat transfer in a concentric annulus. Waves in Random and Complex Media, 2022, pp. 1–25.
[28] N.K. Manna, N. Biswas, D.K. Mandal, U. Sarkar, H.F. Öztop, N. Abu-Hamdeh, Impacts of heater-cooler position and Lorentz force on heat transfer and entropy generation of hybrid nanofluid convection in quarter-circular cavity, Int. J. Numer. Methods Heat. Fluid. Flow. 33 (2023) 1249–1286.
[29] D. Chatterjee, N. Biswas, N.K. Manna, S. Sarkar, Effect of discrete heating-cooling on magneto-thermal-hybrid nanofluidic convection in cylindrical system, Int. J. Mech. Sci. 238 (2023) 107852.
[30] D. Chatterjee, N. Biswas, N.K. Manna, D.K. Mandal, A.J. Chamkha, Magneto-nanofluid flow in cylinder-embedded discretely heated-cooled annular thermal systems: conjugate heat transfer and thermodynamic irreversibility, J. Magn. Magn. Mater. 569 (2023) 170442.
[31] B.M. Al-Srayyih, A. Al-Manea, K. Saleh, A.M. Abed, Q.R. Al-Amir, H.K. Hamzah, F. H. Ali, R. Al-Rbaihat, A. Alahmer, Simulation investigation of the oscillatory motion of two elliptic obstacles located within a quarter-circle cavity filled with Cu-Al2O3/water hybrid nanofluid, Applications (2023) 1–25.
[32] Q.R. Al-Amir, H.K. Hamzah, F.H. Ali, M. Hatami, W. Al-Kouz, A. Al-Manea, R. Al-Rbaihat, A. Alahmer, Investigation of natural convection and entropy generation in a porous titled Z-staggered cavity saturated by TiO2-water nanofluid, Internat. J. Thermofluids 19 (2023) 100395.
[33] N. Biswas, D. Chatterjee, S. Sarkar, N.K. Manna, Magneto-nanofluidic thermal transport and irreversibility in semicircular systems with heated wavy bottom under constant fluid volume and cooling surface constraints, Int. J. Numer. Methods Heat. Fluid. Flow. (2024).
[34] Z. Al-Dulaimi, H.T. Kadhim, M.F. Jaffer, A. Al-Manea, R. Al-Rbaihat, A. Alahmer, Enhanced conjugate natural convection in a corrugated porous enclosure with Ag-MgO hybrid nanofluid, Internat. J. Thermofluids 21 (2024) 100574.
[35] S.S. Akbar, M. Mustafa, Coupled heat and mass transfer to viscoelastic fluid flow in a rotating frame using series and numerical solutions, Int. J. Heat. Fluid. Flow. 106 (2024) 109294.
[36] B. Ozerdem, M. Toksoy, An experimental study of convective heat transfer in a partially filled and horizontally rotating cylinder, Internat. Communicat. Heat Mass Transfer 20 (4) (1993) 579–584.
[37] J. Karcz, M. Major, An effect of a baffle length on the power consumption in an agitated vessel, Chem. Eng. Process. 37 (1998) 249–256.
[38] H. Ma, L. Yin, W. Zhou, X. Lv, Y. Cao, X. Shen, W. Lu, Measurement of the temperature and concentration boundary layers from a horizontal rotating cylinder surface, Int. J. Heat. Mass Transf. 87 (2015) 481–490.
[39] Z. Salman, F. Aiss, M. Almudhaffar, Experimental study of mixed convection in a cavity with a rotating cylinder, J. Adv. Res. Fluid Mech. Thermal Sci. 74 (2) (2020) 16–26.
[40] Y.C. Shih, J. Khodadadi, K.H. Weng, A. Ahmed, Periodic fluid flow and heat transfer in a square cavity due to an insulated or isothermal rotating cylinder, (2009).
[41] K. Wu, F. Huang, J. Shen, A new class of higher-order decoupled schemes for the incompressible Navier-Stokes equations and applications to rotating dynamics, J. Comput. Phys. 458 (2022) 111097.
[42] S.H. Menon, J. Mathew, J. Jayaprakash, Derivation of Navier–Stokes equation in rotational frame for engineering flow analysis, Internat. J. Thermofluids 11 (2021) 100096.
[43] F. Ali, S. Murtaza, N.A. Sheikh, I. Khan, Heat transfer analysis of generalized Jeffery nanofluid in a rotating frame: atangana–Balaenu and Caputo–Fabrizio fractional models, Chaos, Solitons Fractals 129 (2019) 1–15.
[44] O. Schenk, K. Gärtner, Solving unsymmetric sparse systems of linear equations with PARDISO, Futur. Gener. Comput. Syst. 20 (3) (2004) 475–487.
[45] P. Wriggers, Nonlinear finite element methods, Springer Science & Business Media, 2008.

[46] F. Verbosio, A. De Coninck, D. Kourounis, O. Schenk, Enhancing the scalability of selected inversion factorization algorithms in genomic prediction, J. Comput. Sci. 22 (2017) 99–108.

[47] M. Bollhöfer, A. Eftekhari, S. Scheidegger, O. Schenk, Large-scale sparse inverse covariance matrix estimation, SIAM J. Scient. Comput. 41 (2019) A380–A401.

[48] M. Bollhöfer, O. Schenk, R. Janalik, S. Hamm, K. Gullapalli, State-of-the-art sparse direct solvers, Parallel Algorithms Computat. Sci. Eng. (2020) 3–33.